ISSN 1063-7761, Journal of Experimental and Theoretical Physics, 2018, Vol. 127, No. 2, pp. 305–315. © Pleiades Publishing, Inc., 2018.
Original Russian Text © A.A. Lundin, V.E. Zobov, 2018, published in Zhurnal Eksperimental'noi i Teoreticheskoi Fiziki, 2018, Vol. 154, No. 2, pp. 354–367.

SOLIDS AND LIQUIDS

Asymptotic Similarity of Time Correlation Functions and Shape of the ^{13}C and ^{29}Si NMR Spectra in Diamond and Silicon

A. A. Lundin[a,*] and V. E. Zobov[b,]**

[a] *Semenov Institute of Chemical Physics, Russian Academy of Sciences, Vorob'evskoe sh. 26, Moscow, 117977 Russia*
[b] *Kirensky Institute of Physics, Federal Research Center "Krasnoyarsk Scientific Center," Siberian Branch, Russian Academy of Sciences, Akademgorodok 50, Krasnoyarsk, 660036 Russia*
**e-mail: ya-andylun2012@yandex.ru*
***e-mail: rsa@iph.krasn.ru*

Received March 31, 2018

Abstract—Based on the proposed theory, we have investigated the shape of the NMR absorption spectra for ^{13}C and ^{29}Si nuclei in diamond and silicon crystals attributable to the internuclear dipole–dipole interaction. In accordance with the available experimental data, we have considered both crystals with a 100% content of magnetoactive isotopes and crystals with a comparatively low dilution by nonmagnetic nuclei. The time correlation functions (the first of which is the Fourier transform of the NMR spectrum) arising in an infinite chain of coupled differential equations are shown to be mutually similar with a slight time delay. The proposed theory allows the spectrum to be calculated analytically. The results obtained agree satisfactorily with the experimental ones. It is noted that the mutual similarity of the time correlation functions is probably a corollary of the development of dynamical chaos in the system

DOI: 10.1134/S1063776118080216

1. INTRODUCTION

The shape of the nuclear magnetic resonance (NMR) absorption spectra or their Fourier transforms, the free-induction decay (FID) signals, has been perhaps the main source of information about the structure of matter, the mobility in it, the electron–nucleus interactions and the electronic structure, the phase transitions, etc. from the first days after the discovery of NMR until the present. This provided very wide applications of NMR from studies in the fields of condensed matter physics and chemistry to biology and medicine [1–4]. Subsequently, the development and perfection of multipulse NMR methods allowed one (when their application was possible) to improve the extraction of topical information by "editing" the spectra and to deepen appreciably its understanding [3].

The first suggestions regarding the shape of the magnetic resonance signals were put forward in the pioneering paper by Bloembergen, Purcell, and Pound [1]. The absorption lines were assumed to be close in shape to two main types of curves: Lorentzian and Gaussian. Lorentzian curves described the spectra emerging in liquids and solid materials with a strong exchange interaction, i.e., the spectra formed in the presence of rapid fluctuations of the local magnetic field produced by the neighbors on some spin. For such systems a Lorentzian spectrum can be obtained, for example, by solving the Bloch equations [2]. In addition, the absorption spectra of magnetically diluted systems in the absence of inhomogeneous broadening have come to be described by Lorentzian curves since the classic paper by P. Anderson [2, 5]. In contrast, a quasi-static distribution of local fields, which was assumed to be realized in ordinary solids, was associated with a Gaussian shape of the spectrum.

The detection of oscillations in the free-induction decay (FID) signals of ^{19}F in CaF_2 [2, 6], a classical test object for the investigation of NMR spin dynamics, became evidence that it is illegitimate to describe the spectra in it by a Gaussian function. This circumstance gave rise to a lot of both theoretical and experimental works (see, e.g., [6–22] and references therein), especially since quite a few new physical facts and peculiarities of the behavior of spin systems were hidden behind it. New nontrivial facts and possibilities have been revealed until now.

For example, abstracting from the applied aspects of NMR listed at the beginning, it should be pointed out that the problem of the NMR spectrum shape is of fundamental importance for statistical physics, because this problem is basically a special case of the central problem of nonequilibrium statistical mechanics—the problem of the establishment of equilibrium in a system of many interacting bodies. In this sense the problem of relaxation to the state of internal equi-

librium of a many-body paramagnetic spin system of solids with a strong spin–spin coupling is one of the most significant, but most difficult problems in magnetic resonance physics and related phenomena (such as, for example, the magnetic part of the neutron scattering by paramagnets, the infrared spectra and dynamics of quadrupole solids (solid hydrogen), etc.). In addition, it should be said that investigating the appearance and growth of spin correlations and their possible subsequent degradation accompanying the complex processes in the multispin system of a sample during the formation of the NMR spectrum (or FID) is essential for the description of many-body correlations. The latter, in, turns, are necessary for the realization of a quantum register (quantum computer), see [23–26].

Previously, we have developed a theory (see [8, 17, 18, 20–22] and references therein) that allows one to understand some of the characteristic features of the processes during the FID formation and to describe quite satisfactorily the NMR spectra in crystals in which each spin has the nearest environment of a large number of approximately equivalent neighbors, in contrast, say, to quasi-one-dimensional systems (fluorite CaF_2 and fluorapatite $Ca_5F(PO_4)_3$, respectively, are examples). However, despite the fact that crystals of the first mentioned type are widespread, quite intensive studies of the shape of the NMR spectra for single crystals with lattices in which each spin is surrounded by a number of equivalent neighbors "intermediate" between large and small ones are also carried out (for more details see below). Diamond and silicon single crystals with similar crystal lattices serve as typical examples (see, e.g., [11, 12, 19, 27–30]). When the studies mentioned above were carried out, single crystals containing various amounts of magnetoactive isotopes of silicon and carbon nuclei, ^{29}Si and ^{13}C, with concentrations up to 100% were specially grown for the experiments. The spectra obtained, especially for some orientations of the external magnetic field with respect to the crystallographic axes, at a 100% content of magnetoactive nuclei pose a challenge to the theory, because they seem to be a case "intermediate" between large and small numbers of equivalent neighbors. In this paper we discuss and interpret these spectra based on the theory being developed. The spectra obtained when magnetoactive nuclei are diluted by the main isotopes ^{28}Si and ^{12}C are also discussed on the same basis.

2. THE HAMILTONIAN AND BASIC EQUATIONS OF THE DYNAMICS OF A NUCLEAR SPIN SYSTEM

The secular part of the internuclear dipole–dipole interactions in nonmetallic diamagnetic solids, which is almost uniquely responsible for the dynamics of the spin system, under NMR conditions is [2]

$$H = \sum_{i>j}\left\{\frac{3}{2}b_{ij}S_{zi}S_{zj} - \frac{1}{2}b_{ij}\mathbf{S}_i\cdot\mathbf{S}_j\right\} = H_{zz}^0 + H_{\text{ex}}$$
$$= \sum_{i>j}\left\{b_{ij}S_{zi}S_{zj} - \frac{1}{4}b_{ij}(S_i^+S_j^- + S_i^-S_j^+)\right\} = H_{zz} + H_{ff}, \quad (1)$$

where $b_{ij} = \gamma^2\hbar(1 - 3\cos^2\theta_{ij})/2r_{ij}^3$, $\mathbf{r}_{ij}$ is the vector connecting spins i and j, θ_{ij} is the angle formed by the vector $\mathbf{r}_{ij}$ with the constant external magnetic field, and $S_{\alpha i}$ is the α component ($\alpha = x, y, z$) of the spin vector operator at site i. Here and below, the energy is expressed in frequency units.

In traditional experiments using magnetic resonance the spin temperature usually exceeds significantly the energy of the Zeeman and other interactions in the spin system. Therefore, as usual, we will restrict our analysis to the time correlation functions (TCFs) in the high-temperature approximation. The equilibrium high-temperature density matrix in a strong constant magnetic field H_0 is described by the expression [2]

$$\rho_0 \propto \left(1 + \frac{\gamma\hbar H_0}{kT}\sum_{j=1}^{N} S_{zj}\right), \quad (2)$$

where k is the Boltzmann constant, T is the temperature, and N is the total number of spins in the sample.

The free-induction decay (FID) signal arising after the application of a $\pi/2$ pulse to an equilibrium nuclear spin system is known [2] to be proportional to the TCF defined in a frame rotating with the Larmor frequency by the relation

$$A_0(t) = \frac{\text{Tr}\{S_x(t)S_x\}}{\text{Tr}\{S_x^2\}} = \frac{\text{Tr}\{S^+(t)S^-\}}{\text{Tr}\{S^+S^-\}};$$
$$A_0(t) = \sum_{n=0}^{\infty} i^{2n}\left(\frac{M_{2n}}{2n!}\right)t^{2n}. \quad (3)$$

Here, $\{M_n\}$ are the moments, i.e., the coefficients of the FID expansion into a series in powers of time, and since the temperature is very high compared to the internuclear dipole–dipole interaction, only the even-order moments are nonzero, while the FID is, thus, an even function of time, $S_x = \sum_{i=1}^{N} S_{xi}$ is the total x spin component of the system. The dependence $S_x(t)$ is specified by the Heisenberg equation

$$\frac{dS_x}{dt} = i[H, S_x] = iLS_x, \quad (4)$$

L is the Liouville operator, N is the total number of nuclear spins in the sample. It was shown in [31] that calculating the FID (3) is completely equivalent to solving a virtually infinite (a dimension of $\sim 10^{23}$) system of differential equations:

$$\begin{aligned}\dot{A}_0(t) &= i\nu_0^2 A_1(t),\\ \dot{A}_1(t) &= i(A_0(t) + \nu_1^2 A_2(t)),\\ &\cdots\cdots\cdots\cdots\\ \dot{A}_n(t) &= i(A_{n-1}(t) + \nu_n^2 A_{n+1}(t)),\\ &\cdots\cdots\cdots\cdots\end{aligned} \tag{5}$$

The system of equations (5) contains TCFs of various (high) orders and reflects the redistribution of spin–spin correlations over the set of many-body TCFs. The initial conditions for system (5) are

$$A_0(0) = 1, \quad A_n(0) = 0, \quad n \geq 1.$$

The functions $\{A_i(t)\}$ are multi-commutator (many-body) TCFs [31]:

$$\begin{aligned}A_i(t) &= \frac{\langle i|S_x(t)\rangle}{\langle i|i\rangle};\\ |i\rangle &= L^i|0\rangle - \sum_{k=0}^{i-1}\frac{\langle k|L^i|0\rangle}{\langle k|k\rangle}|k\rangle; \quad |0\rangle = |S_x(0)\rangle.\end{aligned} \tag{6}$$

Here, by tradition, the ith degree of the Liouville operator is the procedure of calculating i commutators:

$$L^i = \underbrace{[H,[H,\ldots[H,\ldots]]]}_{i}. \tag{7}$$

In the above expressions the angular brackets denote the calculation of a statistical average, which simply means the calculation of a trace due to the adopted high-temperature approximation [2, 31]. The parameters $\{\nu_n^2\}$, whose properties determine the solution of the system, are uniquely related to the absorption line moments [31]. For the reader's convenience we will give the expressions for several first coefficients:

$$\nu_0^2 = M_2 = \frac{9}{4}\sum_j b_{ij}^2, \quad \nu_1^2 = \frac{M_4 - M_2^2}{M_2},$$

$$\nu_2^2 = \frac{M_2M_6 - M_4^2}{(M_4 - M_2^2)M_2}.$$

Here and below, we assume the nuclear spin to be $S = 1/2$ without any loss of generality [32].

3. MUTUAL SIMILARITY OF MULTISPIN TIME CORRELATION FUNCTIONS AND THE FID SHAPE

Speaking in the language of multiple-quantum (MQ) NMR that has developed over the last 20–25 years and gained wide recognition and acceptance, the system of equations (5) reflects the transfer of single-spin single-quantum coherence $A_0(t)$ to multispin single-quantum coherences [3, 32] (functions $\{A_i(t)\}$) or, in other words [32], the spreading of a gas of correlations over one-dimensional Liouville space whose points are the numbers of the corresponding coherences (time correlation functions). Indeed, the initial order transferred to the spin system in the form of a magnetization directed along the x axis is spread over higher-order TCFs, redistributing among them.

As was shown in [21], the following relation is valid for the TCF $A_2(t)$ from system (5) under some additional conditions (a large number of neighbors surrounding the spin in the lattice (for a further discussion, see below)):

$$A_2(t) \approx \alpha A_0(t + \tau(t)), \tag{8}$$

where α is the number to be determined below, $\tau(t)$ is the function that satisfies the condition $\tau(t) \to 0$ as $t \to \infty$. Hence we assume that the TCF $A_2(t)$ is completely similar to the FID at long times, slightly differing at short ones. The latter is obviously related to different initial conditions for $A_0(t)$ and $A_2(t)$ from system (5). The surge in amplitude $A_2(t)$ from zero to its final value occurs with a slight delay relative to $t = 0$ [32] and, thus, the TCFs $A_0(t)$ and $A_2(t)$ are similar, given this delay. Thus, at small $\tau(t)$ from Eq. (5) we will obtain the expression

$$A_2(t) = \alpha A_0(t) + \alpha\dot{A}_0(t)\tau(t), \tag{9}$$

which reflects the mutual similarity of the TCFs with the delay $\tau(t)$.

Using system (5) and directly comparing the expansions of the functions $A_0(t)$, $A_1(t)$, and $A_2(t)$ into series in powers of t, it is easy to verify that the first term of the expansion of the function $A_2(t)$ into a power series is $t^2/2$, which, in view of relation (9), uniquely determines the choice of the function $\tau(t)$:

$$\tau(t) = 1/\nu_0^2 t. \tag{10}$$

Concurrently, relation (10) also ensures that the second moment of the absorption spectrum (the first sum rule) is correct. Next, let $\alpha = \beta/\nu_1^2$. Here, β is the numerical parameter to be determined below. The similarity law (9) now transforms system (5) to a closed equation:

$$\begin{aligned}\ddot{A}_0(t) + (\beta/t)\dot{A}_0(t) + (\beta + 1)\nu_0^2 A_0(t) = 0,\\ A_0(0) = 1.\end{aligned} \tag{11}$$

In accordance with [33, 34], the physically justified solution of Eq. (11) decaying with time for $\beta > 0$ is

$$A_0(t) = C_1\frac{J_\lambda(\sqrt{\beta + 1}\nu_0 t)}{(\sqrt{\beta + 1}\nu_0 t)^\lambda} = C_1\frac{J_\lambda(bt)}{(bt)^\lambda}, \tag{12}$$

where $(2\lambda)^2 = (\beta - 1)^2$ [33].

The fundamental possibility of expressing the higher-order TCFs via the lower-order ones goes back to the widely known ideas put forward in Bogolyubov's works. On the other hand, the success of the pair interaction model [35, 36] in describing the FID signals of crystals with a large number of spins in the environment of an isolated (any) spin can be assumed to be a corollary of the decay of the higher-order TCFs in (5) into single-spin and pair coherences, which probably

allows the higher-order coherences to be reconstructed via the set of mentioned lower-order ones.

It should be noted that the decaying solution (12) is valid for positive values of λ and $\beta + 1$; J_λ is a Bessel function of order λ; C_1 is the normalization constant providing the initial conditions for the system of equations (5), $C_1 = 2^\lambda\Gamma(\lambda + 1)$ [33]. Although the functional dependence of the decaying solution of Eq. (11) in any case is defined by Bessel functions, their specific choice is determined by the signs of the last two terms in Eq. (11) and the relationship between the constants. For example, if the last term has a negative coefficient, then the solution will be expressed via Macdonald functions $K(t)$ and there will be no oscillations in the solution [33, 34]. The frequency Fourier spectrum of the function (12) is described by the expression

$$g_0(\omega) = \frac{\Gamma(\lambda+1)}{b\sqrt{\pi}\Gamma(\lambda+0.5)}\left(1-\frac{\omega^2}{b^2}\right)^{(2\lambda-1)/2}, \qquad (13)$$

at $|\omega| < b$; at $|\omega| > b$ we obtain $g_0(\omega) = 0$. Thus, the spectrum specified by Eq. (13) is truncated at a fixed frequency. Here, $\Gamma(x)$ is the gamma function, while the spectral component (13) is normalized to unity:

$$\int_{-\infty}^{\infty} g_0(\omega)d\omega = 1.$$

The spectral moments of the function (13) are determined from the formula

$$M_{2n} = \frac{1}{2^{2n}}\frac{b^{2n}(2n)!\Gamma(\lambda+1)}{n!\Gamma(\lambda+n+1)}. \qquad (14)$$

For our case where the solution of Eq. (11) is expressed via Bessel functions $\{J_\lambda(t)\}$, the parameters of the equation and, accordingly, the order of the Bessel functions can be expressed via the excess of the spectrum, $\varepsilon = M_4/M_2^2$, using relation (14):

$$\beta = \frac{3\varepsilon-3}{3-\varepsilon}, \quad \lambda = \frac{2\varepsilon-3}{3-\varepsilon}. \qquad (15)$$

Note that Eq. (15) contains only two parameters and, therefore, only two moments (the first and second sum rules) are sufficient for their determination. Of course, it does not follow from the foregoing that the remaining moments of the spectrum are absent. They are expressed via the above ones in accordance with the derived functional dependence. Finally, note that the constants $\{\nu_j\}$ in the system of equations (5) are frozen very rapidly ($\nu_j = \nu_k$ for all $j > k$) with increasing number j when calculating the contributions to the spectrum from the spins of the nearest environment (the cell, see below) of some isolated spin [20, 21], which allows us to restrict ourselves to the lowest-order moments in this situation.

Now, to compare the described theory with the available experimental results, it is appropriate to use the model of separation of the local magnetic field produced by the internuclear dipole–dipole interaction (1) into two components proposed and justified by us previously [8, 35, 36]. The basic proposition of this model is that due to the high (compared to the interaction) temperature, the local magnetic field acting on some marked (any) nuclear spin in a crystal can be represented as the sum of two statistically independent contributions of a fundamentally different nature with respect to the correlations existing in the spin system. We emphasize that here we are talking exclusively about the time correlations and the correlation of the field acting on the spin with the spin itself. This means that a change in the orientation of the marked spin entails a change in the field acting on it with a slight delay. Such correlations in the spin system, suggesting that the spin, in a sense, acts "on itself," twisting its neighbor, occur only due to the presence of the flip-flop term H_{ff} (or, in different notation, the scalar term H_{ex}) in the Hamiltonian (1), because otherwise, when only the H_{zz} interaction remains, the motion of the marked spin does not affect in any way the field acting on it. The action of the term H_{ff} contained in (1) is realized in the spin system in the form of flip–flop processes (FFPs), whose probability, in accordance with the results from [8, 35, 36], is determined by a rapidly converging ($\propto 1/r^6$) function of the distance between rotating spins. The spins with which the FFP probability is great (relative to other spins) move in a correlated way with the isolated spin in the above sense. However, the number of such spins cannot be too large because of the rapid convergence (depending on the distance) of the FFP probability. For example, in single crystals of fluorite (CaF_2), a classical object for the studies of NMR spin dynamics, the radii of the regions in which there is a correlated motion of spins (the "self-action" of the marked spin) for three principal orientations of the constant magnetic field are [8, 35, 36] [100] $\leftrightarrow d$, [110] $\leftrightarrow 2^{1/2}d$, and [111] $\leftrightarrow 3^{1/2}d$, where d is the ^{19}F lattice constant in CaF_2.

The crystal region with the center on the isolated spin and a radius equal to the radius of the above correlations was called a cell [8, 35, 36]. Next, it was shown in the mentioned papers that the contribution to the FID from the spins outside the cell could be described at comparatively short times by a Gaussian random function. Thus, the presence of two contributions to the local field is determined by the presence of two regions in the crystal, in one of which the spins move in a correlated way in the above sense with the marked spin, while in the other region they don't. It is worth noting that in practice the approximations in [8, 36, 36], just as in other papers using the concept of a cell, are an expansion in terms of the inverse number of spins in the cell Z.

The decomposition of the local field (ω in frequency units) on some marked spin into two components, $\omega = \omega_1 + \omega_2$ (ω_1 from the nearest neighbors

(cell) and ω_2 from the more distant spins (distant environment), allowed the characteristic features of the FID in a solid to be explained. Indeed, let ω_1 and ω_2 be two statistically independent contributions to the random local field with distribution functions in the form of a rectangle ($P_1(\omega_1)$ and a Gaussian function ($P_2(\omega_2)$), respectively. Then, $P(\omega) = P_1(\omega_1)P_2(\omega_2)$ and, as a result, for the FID we obtain

$$G(t) = \int_{-\infty}^{\infty} e^{i\omega t} P(\omega) d\omega = \int_{-\infty}^{\infty} e^{i\omega_1 t} P_1(\omega_1) d\omega_1$$
$$\times \int_{-\infty}^{\infty} e^{i\omega_2 t} P_2(\omega_2) d\omega_2 = \frac{\sin bt}{bt} \exp\left(-\frac{a^2 t^2}{2}\right)$$

Abraham's trial function that describes well the experiment, at least at moderately long times [2, 37].

The FID component due to the spins of the distant environment is a function monotonically decaying with time. In accordance with the theory developed in [8, 35, 36], it can be described based on Anderson's statistical theory [2], in contrast to the FID component produced by the cell spins. Thus, remaining Gaussian at short times, it is transformed to the following function at times $T_2^* > 3T_2$ (T_2 is the characteristic time of spin–spin interactions) [8, 35] due to the FFP spins of the distant environment:

$$A_{0(\text{ext})}(t) = \exp\left\{-a^2 \int_0^t (t-\tau) k(\tau) d\tau\right\}. \quad (16)$$

As in experimetntal results [37], at times shorter than the time of correlation of $k(\tau)$, Eq. (16) gives a Gaussian function of time and a simple exponential function at longer times. All of the characteristic parameters and times in Eq. (16) for fluorite were calculated in [8, 35, 36] and are in good agreement with the experimental results [37].

4. COMPARISON OF THE THEORY WITH EXPERIMENTAL RESULTS

Most of the goal-oriented detailed studies of the NMR line shape in solid dielectrics were carried out on ^{19}F nuclei in fluorite CaF_2, a distinct ionic crystal. In this crystal only the fluorine nuclei forming a simple cubic lattice possess a magnetic moment (the main calcium isotope has zero spin). As a model object CaF_2 is attractive by the comparative ease of obtained the NMR signal from it and by the simplicity of its crystal structure. However, the question of how general the characteristic features of the absorption line shape and the FID signal detected in CaF_2 are is of indubitable interest.

For the subsequent discussion it is appropriate to note that the above relations (5)–(15), in principle, are actually absolutely formal and were written out irrespective of the physical model presented above [8, 35, 36]. Passing to the model implies substituting the value of the constant ν_0 calculated for the cell into relations (5)–(8): $\nu_0^2 = M_2'$, where M_2' is the contribution to the second moment from the cell spins, and subsequently using the similarity law (6) with a specific choice of the constant β. Below the FID component of interest to us, which is determined by the cell spins, will be denoted by $A_{0(\text{int})}(t)$. Thus, for example, the FID for the entire crystal in the adopted notation takes the form

$$A_0(t) = A_{0(\text{init})}(t) A_{0(\text{ext})}(t). \quad (17)$$

We have noted above (Eq. (15)) that β (and, consequently, the order λ of the Bessel function) can be easily related to the excess ε of the FID component produced by the cell spins. For its calculation we need to determine the contribution to the fourth moment from the cell spins. When estimating it, in order not to calculate the cumbersome lattice sums, which was done in [8, 35] for CaF_2, below, for simplicity, we will neglect the deviation of the function $A_{0(\text{ext})}(t)$ from the Gaussian one in our calculations of the NMR spectra for diamond and silicon. Such an estimate will not introduce a significant error into the calculations. Denoting the fourth moment of the cell by M_4', we will find

$$M_4' = M_4 - 3M_{2(\text{ext})}^2 - 6M_2' M_{2(\text{ext})}. \quad (18)$$

Here, $M_{2(\text{ext})}$ is the second moment of the function $A_{0(\text{ext})}(t)$.

In CaF_2 single crystals for external field orientations in the [100] and [110] directions the values of ε for the cell are 1.75 and 1.88, respectively. It is appropriate to round them off to 1.8, which leads to $\lambda = 0.5$ and $\beta = 2$. Here we treated the rounding-off rules somewhat freely. However, since at each fixed value of the argument the Bessel functions are entire functions of their order λ, it can be assumed that the rounding-off will not affect significantly the results of our calculations. At the same time, for example, in the case under consideration, the rounding-off makes it possible to work with Bessel functions of half-integer orders expressed via elementary functions. Thus, for these orientations, in accordance with Abraham's trial function, from Eq. (12) [21] we will obtain

$$A_{0(\text{init})}(t) = \frac{C_1 J_{1/2}(\sqrt{3}\nu_0 t)}{(\sqrt{3}\nu_0 t)^{1/2}} = \frac{\sin(\sqrt{3}\nu_0 t)}{\sqrt{3}\nu_0 t}, \quad (19)$$

the parameter b calculated using with the recipe described in [8, 35], according to which $\sqrt{3}\nu_0 = \sqrt{3M_2'}$ (where M_2' is the contribution to the second moment of the spectrum from the cell spins), is in remarkable agreement with all of the available experimental results [37]. One of the examples of a completely different crystal structure is stretched crystalline polyethylene

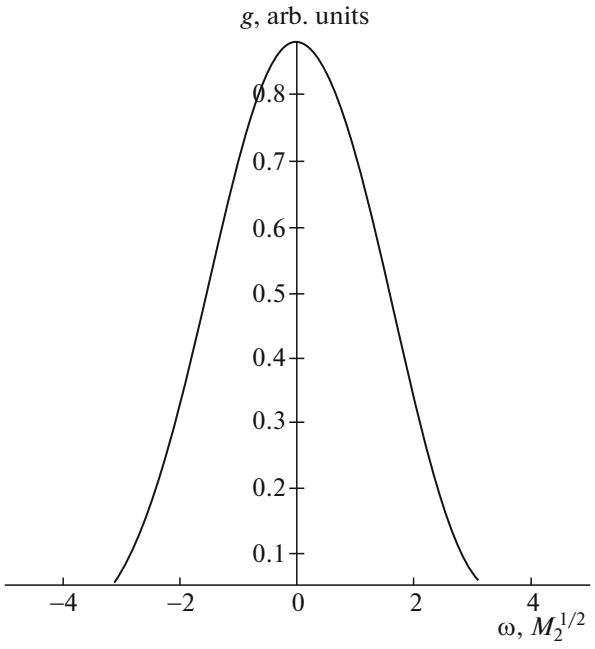

Fig. 1. NMR spectrum of a diamond/silicon lattice at a magnetoactive-isotope concentration $C = 1$. The external magnetic field is directed along the [100] axis. The frequency in units of $M_2^{1/2}$ is along the horizontal axis. The amplitude g is along the vertical axis. The excess of the cell including eight spins for this orientation is $\varepsilon = 2.03$. The order of the Bessel function is $\lambda = 1.09$.

in the form of a trans-zigzag. For the cell spins in crystalline polyethylene with a field orientation along the molecule axis the calculated $\varepsilon = 1.83$ should be rounded off to 1.8; as a consequence, for the corresponding FID component we will obtain Eq. (19). Note that apart from this, the authors of [38] adequately described the oscillating FID component in polyethylene by the function (19) for external magnetic field orientations not only along the molecule axis, but also perpendicularly and at an angle of 45° to it. However, in all cases, the authors of [38] (in contrast to us) use the function (19) simply as an empirical trial function by selecting the parameter b from experimental data. Note that as the orientation of the external magnetic field changes with respect to the crystallographic axes, the pattern (structure) of the internuclear dipole–dipole interaction changes due to the angular dependence of the Hamiltonian (1). For example, for a field orientation in the [111] direction in CaF_2, it is appropriate to round off $\varepsilon = 2.2$ to $\varepsilon \approx 2$ and we will obtain $\lambda = 1$ and, accordingly, $\beta = 3$. The function $J_1(2\nu_0 t)/(2\nu_0 t)$ arising in this case describes excellently the oscillatory FID component observed experimentally for this orientation (see Fig. 1 from [21]). Among other studies of the shape of the spectra in ionic crystals we can note the results obtained in cubic single crystals with various types of lattices (LiF, NaF, NaCl, CsF, SrF_2, and BaF_2) with two kinds of nuclear spins, where NMR was observed on each kind of nuclei [10, 39, 40]. The FID signals observed in them are also described by Eq. (17); the oscillating component is still described satisfactorily by Eq. (19), while the Gaussian–exponential (Anderson) component specified by Eq. (16) is now determined not only by the spins of the distant environment, but also by all (including the nearest neighbors) spins of another kind. Thus, if the resonance in LiF is observed on ^{19}F nuclei, then all lithium spins contribute to the Anderson component.

If a crystal contains isolated groups of spins (for example, methyl groups, pairs of water protons, etc.), then the isolated group is chosen as a cell [8]. Its spectrum usually has a fine structure and is, in a sense, unique. To clarify the question about the universality of describing the spectra of three-dimensional crystals containing no isolated groups of spins (for example, crystalline hydrates with significantly isolated pairs of water protons) based on the presented model and, accordingly, Eqs. (9), (12), (13), and (17), obviously, we should study the NMR line shape and the FID signals in more complex crystal structures than the cubic one, whose emergence is attributable to a type of interaction noticeably different from that responsible for the existence of a lattice in the CaF_2 single crystal. One of such examples, single-crystal polyethylene, has already been discussed above. We discussed the spectra of some molecular crystals (naphthalene and anthracene) in [22].

Below we will discuss the ^{13}C and ^{29}Si spectra in diamond and silicon single crystals, beginning with crystals with a 100% content of magnetoactive isotopes. It is worth noting that predominantly the absorption spectra rather than the FID signals are given in the experimental works [11, 12, 27–30]. The nearest environment of each of the nuclei in these structures enters into the tetrahedron of four spins (see Fig. 1 from [27] and Fig. 1 from [30]) whose interaction with the central spin depends significantly on the external magnetic field orientation due to the angular dependence of the Hamiltonian (1) (see Tables 1–3). Because of this, more distant spins can also make a significant contribution.

Tables 1–3 demonstrate the influence of the geometric factor on the formation of the ^{13}C and ^{29}Si NMR spectra in diamond and silicon. The edge length of the lattice constant is taken to be 2, n is the number of spins that have the same interaction with the "isolated" (central) spin of the cell due to the geometric factors.

As follows from Table 1, for an external magnetic field orientation in the [100] direction eight spins turn out to be approximately equivalent neighbors interacting relatively strongly with the central spin (and, hence, entering into the cell). The remaining spins of the crystal contribute to the TCF $A_{0(\text{ext})}(t)$, which, for simplicity, we assumed to be Gaussian. The total second moment of the spectrum was taken to be unity.

The fraction of the total second moment accounted for by the cell spins and the distant environment was 0.487 and 0.513, respectively. The excess of the spectral component of the cell calculated from the formula

$$\varepsilon_{\text{int}} = M_4'/M_2' \tag{20}$$

for this orientation turned out to be approximately 2.03, the parameter β was 3.19, and the order of the Bessel function λ in relation (12), according to Eq. (15), was 1.09. Subsequently, as follows from Eq. (17), the Fourier cosine transform of the product of functions was performed to obtain the spectrum. The results presented in Fig. 1 agree well with the experimental spectra in diamond and silicon (cf. Fig. 2 from [11] and Fig. 2 from [28]).

For an external magnetic field orientation in the [110] direction four spins turn out to be approximately equivalent neighbors entering into the cell (Table 2). The fraction of the second moment accounted for by the cell and the distant environment was 0.813 and 0.187, respectively. The excess of the spectral component of the cell calculated from Eq. (20) for this orientation is 1.832, $\beta = 2.137$, and the order of the Bessel function is $\lambda = 0.567$. The spectra presented in Fig. 2 agree well with the experimental ones (cf. Fig. 2 from [11] and Fig. 2 from [28]).

For an external magnetic field orientation in the [111] direction the interaction with one of the nearest neighbors exceeds noticeably the interaction with the remaining near spins and is 0.635 in fractions of the second moment. If only this neighbor is taken into account as a "cell," then the spectrum turns out to be in the form of a pronounced Pake doublet. Supplementing the cell by three more nuclei (see Table 3) enhances the resolution quite noticeably and deepens the doublet dip. In this case, the fraction of the second moment accounted for by the cell spins and the Gaussian function becomes 0.847 and 0.153, respectively. The excess calculated from Eq. (20) turned out to be 1.303, while the order of the Bessel function was $\lambda = 0.232$. The results of our calculations for the Pake doublet and the calculations using Eq. (13) are presented in Fig. 3. As can be seen from a comparison of the computed curves with the experimental ones (Fig. 2 from [11] and Fig. 2 from [28]), the result obtained when only one neighbor is included in the cell corresponds better to the experiment.

Apart from the foregoing, for the silicon and carbon crystals being discussed we investigated the NMR spectra obtained by diluting the magnetoactive isotope (reducing its concentration) [28–30]. For a low dilution, when the number of magnetoactive nuclei varied near 90%, the spectra were virtually indistinguishable from those of an undiluted crystal. As would be expected, for a significant dilution, in accordance with the universally accepted views, the spectra narrowed, transforming into Lorentzian curves (exponential FIDs). To study the qualitative transformation of the spectrum, we will also

Table 1. Dimensionless dipole–dipole interaction constants for an external field orientation in the [100] direction

n	r^2	$3\cos^2\vartheta - 1$	$(1/r^6)(3\cos^2\vartheta - 1)^2$
4	3/4	0	0
4	11/4	16/11	$(4/11)^3(16/11)^2 = 0.1017$
8	11/4	−8/11	$(4/11)^3(8/11)^2 = 0.0254$
4	2	−1	$(1/2)^3 = 0.125$
8	2	1/2	$(1/2)^3(1/2)^2 = 0.03125$
2	4	2	$(1/4)^3 2^2 = 0.0625$
4	4	−1	$(1/4)^3 = 0.0156$

apply the model presented above for concentrations C less than unity. In this case, Eq. (11) was used to calculate the FID. We still set the second moment equal to 1 and determined the excess of the spectrum dependent on the concentration using the formula

$$\varepsilon(C) = \frac{M_4(C)}{M_2^2(C)} = \frac{7}{3} + \left(\frac{1}{C} - \frac{7}{3}\right) S_2 + \frac{2}{3} S_3,$$
$$S_2 = \sum_k b_{jk}^4 \Big/ \left(\sum_k b_{jk}\right)^2, \tag{21}$$
$$S_3 = \frac{1}{N} \sum_{jkl} b_{jk}^2 b_{jl} b_{kl} \Big/ \left(\sum_k b_{jk}\right)^2.$$

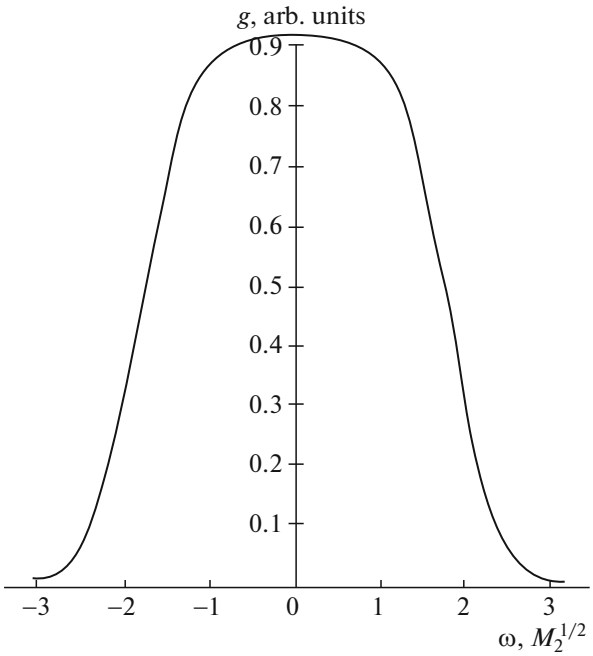

Fig. 2. NMR spectrum of a diamond/silicon lattice at a magnetoactive-isotope concentration $C = 1$. The external magnetic field is directed along the [110] axis. The excess of the cell containing four spins for this orientation is $\varepsilon = 1.832$. The order of the Bessel function is $\lambda = 0.567$.

Table 2. Dimensionless dipole–dipole interaction constants for an external field orientation in the [110] direction

n	r^2	$3\cos^2\vartheta - 1$	$(1/r^6)(3\cos^2\vartheta - 1)^2$
2	3/4	−1	$(4/3)^3 = 2.370$
2	3/4	1	$(4/3)^3 = 2.370$
2	11/4	−1	$(4/11)^3 = 0.0481$
6	11/4	−5/11	$(4/11)^3(5/11)^2 = 0.0099$
4	11/4	13/11	$(4/11)^3(13/11)^2 = 0.0672$
2	2	2	$(1/2)^3 2^2 = 0.5$
2	2	−1	$(1/2)^3 = 0.125$
8	2	−1/4	$(1/2)^3(1/4)^2 = 0.0078$
2	4	−1	$(1/4)^3 = 0.0156$
4	4	1/2	$(1/4)^3(1/2)^2 = 0.0039$

Table 3. Dimensionless dipole–dipole interaction constants for an external field orientation in the [111] direction

n	r^2	$3\cos^2\vartheta - 1$	$(1/r^6)(3\cos^2\vartheta - 1)^2$
1	3/4	2	$(4/3)^3 2^2 = 9.4815$
3	3/4	−2/3	$(4/3)^3(2/3)^2 = 1.0535$
3	11/4	−10/11	$(4/11)^3(10/11)^2 = 0.0397$
3	11/4	14/11	$(4/11)^3(14/11)^2 = 0.0779$
6	11/4	−2/11	$(1/11)^3(2/11)^2 = 0.0016$
6	2	1	$(1/2)^3 = 0.125$
6	2	−1	$(1/2)^3 = 0.125$
6	4	0	0

Table 4. Values of the lattice sums used in Eq. (21) (from [41]) and values of the excess for diamond/silicon lattices for the principal external magnetic field orientations (from [12])

External magnetic field orientation	S_2	S_3	ε
[100]	0.147	0.380	2.3906
[110]	0.169	0.201	2.2419
[111]	0.419	0.0121	1.7822

The numerical values of the lattice sums in Eq. (21) and the values of the excess at $C = 1$ taken from [41] for diamond/silicon lattices for various external magnetic field orientations are given in Table 4. It should be emphasized that in the third term of Eq. (11) the factor $(\beta + 1)$ was also multiplied by C. The parameter β was determined from the excess using Eq. (15). The results of our calculations for $C = 0.8$ and 0.5 for external magnetic field orientations in the [100] and [111] directions are presented in Figs. 4 and 5, respectively. The spectrum is seen to narrow; the doublet characteristic for the [111] orientation collapses. Note that here and below we will abstract from the effects related to the doping of silicon crystals with impurities (for example, phosphorus).

A different way of choosing the parameter β is needed for a significantly reduced concentration and an excess exceeding 3, because in the above-described approach the solution of the equation becomes divergent and the description of a diluted spin system on this basis loses its meaning. Although the spectrum specified by Eq. (13) actually narrows as the order of the Bessel function λ increases, its transformation occurs through a Gaussian-like curve whose wings are still truncated in accordance with this formula. For large λ we have

$$g_0(\omega) \propto \exp\left[-\frac{\omega^2}{(b/\sqrt{\lambda})^2}\right], \quad \text{for} \quad |\omega| < b; \qquad g_0(\omega) = 0 \quad \text{for} \quad |\omega| > b. \tag{22}$$

As the excess in the denominator of formula (15) approaches 3, which corresponds to the excess of a "true Gaussian function," the formula, along with relation (12) expressing the solution via Bessel functions $\{J_\lambda\}$, loses its meaning. From the viewpoint of a "physical picture," this probably implies that the concept of a cell becomes meaningless and the crystal spectrum should be considered without isolating the latter.

Thus, if we attempt to describe the further narrowing of the spectrum using an equation like Eq. (11), it probably makes sense to properly change the signs in front of the terms in Eq. (11) somewhere near the limiting point. Its decaying solutions will then be expressed via Macdonald functions $K(t)$ close in form to a simple exponential function [21, 33, 34]. As is well known, neither the second moment nor higher-order moments can be determined for Lorentzian curves [2]. In this approach the numerical coefficients β in front of the terms should also be changed in a reasonable way. Since for Gaussian-like functions the half-width is close to the square root of the second moment, it is appropriate to replace ν_0^2 by the square of the spectrum half-width [2] $\Delta \approx 3.8\gamma^2\hbar C$. Equation (11) is now transformed to

$$\ddot{A}_0(t) - \frac{\beta}{t}\dot{A}_0(t) - (\beta + 1)\Delta^2 A_0(t) = 0, \qquad \beta > 0, \quad A_0(0) = 1. \tag{23}$$

Here, C is the dimensionless concentration. Next, it is easy to verify that, in principle, for a properly chosen parameter β the spectrum will actually become "Lorentz-like."

5. DISCUSSION

At first glance, the universality of the FID description based on the above-described model of a cell in

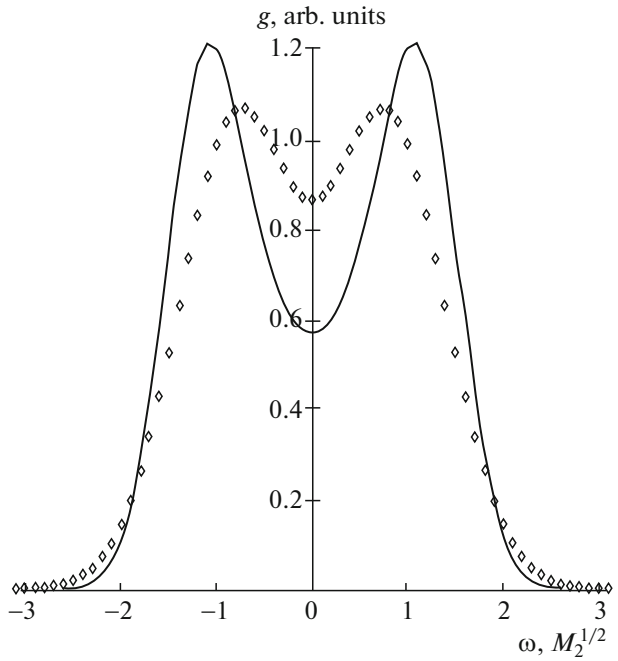

Fig. 3. NMR spectrum of a diamond/silicon lattice at a magnetoactive-isotope concentration $C = 1$. The external magnetic field is directed along the [111] axis. The rhombs indicate the case where only one nearest neighbor enters into the cell (Pake doublet). The solid curve indicates the case where four neighbors enter into the cell (see Table 3). The excess of the cell for this choice of the cell (four neighbors) is $\varepsilon = 1.3$; the order of the Bessel function is $\lambda = 0.232$.

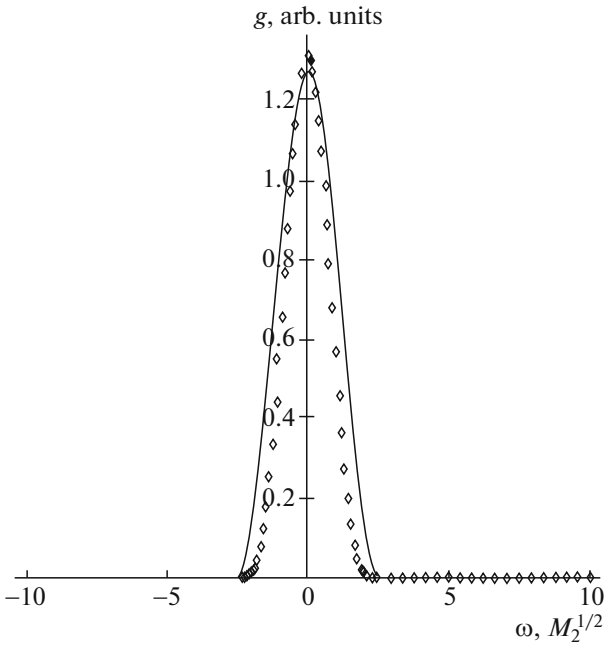

Fig. 4. Narrowing of the spectra for a field orientation along [100] in silicon/diamond crystals with a magnetic dilution. The solid curve represent the dimensionless concentration $C_1 = 0.8$. The excess is $\varepsilon(C_1) \approx 2.43$, the order of the Bessel function is $\lambda(C_1) \approx 4.49$. The rhombs represent the concentration $C_2 = 0.5$. The excess is $\varepsilon(C_2) \approx 2.54$, the order of the Bessel function is $\lambda(C_2) \approx 3.24$.

materials with such a diverse structure as, for example, polyethylene and fluorite (CaF_2) creates a rather strange impression. The structures of the crystals with diamond lattices investigated here and some of the molecular crystals considered in [22] also differ significantly from the ionic ones listed above, while the polymer chain of polyethylene more likely resembles the one-dimensional system of fluorines in fluorapatite $Ca_5F(PO_4)_3$ [42], in which the line is an allowed triplet, than the simple cubic lattice of fluorite. As follows from the foregoing, the shape of the NMR spectrum, in general, may not possess pronounced differences for crystal structures of various types. The only common element of the structures listed above is a relatively large number of spins in the cell Z (approximately equivalent nearest neighbors). In this case, as can be seen from the example with polyethylene, $Z = 3$ is a "large" number in this sense. In fluorapatite the ^{19}F nuclei form isolated linear chains, $Z = 2$, and the cell turns out to be impossible to isolate efficiently. At the same time, if the spin enters into a significantly isolated group for "geometrical reasons" (for example, crystalline hydrates, methyl groups in some compounds, the situation emerging when the field is oriented in the [111] direction in diamond-type lattices, etc.), then the cell isolation turns out to be self-evident and possible. Note that if the cell isolation is possible, then its contribution to the spectrum turns out to be truncated at the frequency determined by the cell sizes.

The probable cause of the functional "universality" of the NMR spectrum shape, its actual independence of the crystal structure (the convolution of a truncated spectral component and a Gaussian-like function), is the development of dynamical chaos in the nuclear spin system that has a homoclinic pattern, because the system is conservative. As follows from the general theory [43–45], a mutual similarity of the various TCFs referring to the same object serves as one of the argument for this. The transformations specified by formulas of like (8)–(10) that are successively applied to the system of equations (5) actually demonstrate the required similarity of the TCFs under some additional conditions. For example, if the TCF $A_4(t)$ is transformed in accordance with these formulas, then we will obtain

$$A_4(t) = \alpha_2 A_2(t) + \alpha_2 A_2(t)\tau_2(t). \qquad (24)$$

Then, when choosing $\tau_2(t) \propto 1/t$, the equation for $A_4(t)$ will coincide in form with Eq. (11), differing in two respects: in accordance with system (5), the constants $\{\nu_j\}$ will be different and the inhomogeneous term $A_0(t)$ will appear. However, as we showed previously [17, 18, 46], the approximation of "frozen constants"

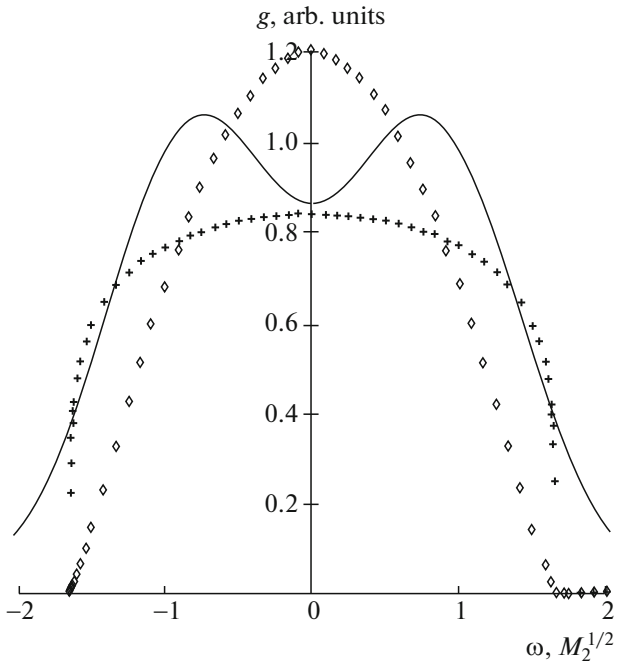

Fig. 5. Narrowing of the spectra for a field orientation along [111] in silicon/diamond crystals with a magnetic dilution. The solid curve represent the dimensionless concentration $C = 1$. Crosses represent the concentration $C_1 = 0.8$. The excess is $\varepsilon(C_1) \approx 1.89$, the order of the Bessel function is $\lambda(C_1) \approx 0.7$. The rhombs represent the concentration $C_2 = 0.5$. The excess is $\varepsilon(C_2) \approx 2.2$, the order of the Bessel function is $\lambda(C_2) \approx 1.76$.

$\{\nu_j\}$ (all $\nu_j = \nu_k$ for $j > k$) is a very good approximation for describing the contribution to the FID from the cell spins even under freezing starting from ν_0 if the number Z is great. Thus, if the constants are frozen, then the transformations (24) and (9) will coincide completely. In contrast, the inhomogeneous term $A_0(t)$ at relatively long times is transformed into a δ function [34] and plays the role of an initial condition. The equation for $A_6(t)$ and so on can be derived in a similar way.

In conclusion, note the paper [13] (see also the references therein), where the long-time asymptotic behavior of the FID for solid xenon enriched by the xenon isotopes 129 and 131 in various concentrations (face-centered cubic lattice) was investigated. The maximum ^{129}Xe concentration reached 85.5%. In addition, the asymptotic behavior of the FID for fluorite and some other TCFs was investigated. As was pointed out in [13], the asymptotic behavior was well described by the universal expression

$$\Gamma(t) \propto \cos(\omega t + \phi)\exp(-ct). \quad (25)$$

Of course, the constants in Eq. (25) for each material and each orientation had their own values. They were selected from an experiment when the asymptotic behavior of TCFs was fitted by the empirical function (25). Note that Eq. (25) slightly differs from the asymptotic behavior of the FIDs measured previously in CaF_2 by Engelsberg and Lowe [37] for the principal crystal orientations with respect to the constant external magnetic field:

$$\Gamma(t) \propto \frac{\sin(bt)}{bt}\exp(-ct). \quad (26)$$

This discrepancy is probably attributable to a slightly less precise processing of the experiment in [13] than in [37]. However, this discrepancy plays no fundamental role for the subsequent discussion.

As was noted in [13], Eq. (25) for the asymptotic behavior of various TCFs probably points to the presence of Pollicott–Ruelle resonances in the closed spin system with a discrete (or, if your wish, quasi-continuous) power spectrum under consideration [17, 18, 43–45]. The presence of such features in the frequency (complex) spectrum of the TCF for a fairly wide set of chaotic dynamical systems was first predicted in [47]. It was shown in [43–45, 47] that in a number of objects of this kind the temporal asymptotic behavior of the TCF is determined by the singular points of its complex frequency spectrum closest to the real axis irrespective of the structure and form of the operators in it. This singular points, along with other, more distant ones, are called the above-mentioned resonances. If this singularities are a simple pole lying at a point of the complex plane $z = \gamma + i\omega$, then the residue at it, usually in the form $\sigma_-(B)\sigma_+(C)$ (where σ_- and σ_+ are the distributions covariant with respect to the time evolution, B and C are the set of operators entering into the TCF), describes the temporal asymptotic behavior of the TCF of interest to us:

$$F(B,C)\exp(-\gamma + i\omega)t + F^+(B,C)\exp(-\gamma - i\omega)t. \quad (27)$$

The presence of such resonances and, accordingly, the asymptotic behavior described by Eqs. (25) and (26), along with the asymptotic similarity of various TCFs arising in our paper from Eqs. (8)–(10) and (24), is the main signature of the development of dynamical chaos in the system. If follows from the theory proposed in this paper (Eqs. (13), (16), (17)) [33] that, irrespective of the crystal structure, the temporal asymptotic behavior of the FID is described by the expression

$$A_0(t) \approx \frac{C_1}{b^\lambda}\sqrt{\frac{2}{\pi t^{1+2\lambda}}}\cos\left(t - \lambda\frac{\pi}{2} - \frac{\pi}{4}\right)\exp(-ct) \quad (28)$$

which corresponds to Eq. (27). Some difference in the pre-exponential factors in Eqs. (25), (26), and (28) may stem from the fact that the Pollicott–Ruelle feature in this case is, for example, a branch point rather than a pole [43–45]. Thus, the development of homoclinic dynamical chaos in the nuclear spin system is probably responsible for the weak dependence of the shape of the NMR absorption spectra (or FIDs) on the object's structure.

ACKNOWLEDGMENTS

We thank V.A. Atsarkin, V.V. Demidov, F.S. Dzheparov, and E.B. Feldman for the discussion of our results. This work was supported by a subsidy allocated by the Institute of Chemical Physics of the Russian Academy of Science for the State assignment, theme 0082-2018-0005, code TSITIS AAAA-A18-118020690203.

REFERENCES

1. N. Bloembergen, E. M. Purcell, and R. V. Pound, Phys. Rev. **73**, 679 (1948).
2. A. Abragam, *The Principles of Nuclear Magnetism* (Clarendon, Oxford, 1961), Chs. 4, 10.
3. R. Ernst, G. Bodenhausen, and A. Wokaun, *Principles of NMR in One and Two Dimensions* (Mir, Moscow, 1990; Clarendon, Oxford, 1987).
4. B. Blumich, *Essential NMR for Scientists and Engineers* (Springer, Berlin, 2005).
5. P. W. Anderson, Phys. Rev. **82**, 342 (1951).
6. I. J. Lowe and R. Norberg, Phys. Rev. **157**, 46 (1957).
7. P. Borckmans and D. Walgraef, Phys. Rev. **167**, 282 (1968).
8. A. A. Lundin and B. N. Provotorov, Sov. Phys. JETP **43**, 1149 (1976).
9. N. V. Zavarnitskii and I. S. Solodovnikov, J. Exp. Theor. Phys. **87**, 546 (1998).
10. V. E. Zobov, M. A. Popov, Yu. N. Ivanov, and A. I. Lifshits, J. Exp. Theor. Phys. **88**, 157 (1999).
11. K. Lefman, B. Buras, E. J. Pedersen, et al., Phys. Rev. B **50**, 15623 (1994).
12. J. Jensen, Phys. Rev. B **52**, 9611 (1994).
13. E. G. Sorte, B. V. Fine, and B. Saam, Phys. Rev. B **83**, 064302 (2011).
14. C. M. Sanchez, P. R. Levstein, R. A. Acosta, and A. K. Chattah, Phys. Rev. A **80**, 012328 (2009).
15. B. Meier, J. Kohlrautz, and J. Haase, Phys. Rev. Lett. **108**, 177602 (2012).
16. S. W. Morgan, V. Oganesyan, and G. S. Boutis, Phys. Rev. B **86**, 214410 (2012).
17. V. L. Bodneva and A. A. Lundin, J. Exp. Theor. Phys. **108**, 992 (2009).
18. V. L. Bodneva and A. A. Lundin, J. Exp. Theor. Phys. **116**, 1050 (2013).
19. F. S. Dzheparov, D. V. Lvov, and M. A. Veretennikov, JETP Lett. **98**, 484 (2013).
20. V. L. Bodneva, A. A. Lundin, and A. A. Milyutin, Theor. Math. Phys. **106**, 370 (1996).
21. A. A. Lundin, J. Exp. Theor. Phys. **83**, 759 (1996).
22. V. O. Zavel'skii and A. A. Lundin, Russ. J. Phys. Chem. B **10**, 379 (2016).
23. V. E. Zobov and A. A. Lundin, J. Exp. Theor. Phys. **103**, 904 (2006).
24. G. A. Bochkin, E. B. Fel'dman, S. G. Vasil'ev, and V. I. Volkov, Appl. Magn. Res. **49**, 25 (2018).
25. S. I. Doronin, E. B. Fel'dman, and F. I. Zenchuk, J. Chem. Phys. **134**, 034102 (2011).
26. V. E. Zobov and A. A. Lundin, J. Exp. Theor. Phys. **120**, 762 (2015).
27. R. Schaumburg, E. Shabanova, and J. P. F. Sellschop, J. Magn. Res., Ser. A **112**, 176 (1995).
28. A. S. Verhulst, D. Maryenko, Y. Yamamoto, and K. Ito, Phys. Rev. B **68**, 054105 (2003).
29. H. Hayashi, K. Ito, and L. Vlasenko, Phys. Rev. B **78**, 153201 (2008).
30. B. Christensen and J. C. Price, Phys. Rev. B **95**, 134417 (2017).
31. F. Lado, J. D. Memory, and G. W. Parker, Phys. Rev. B **4**, 1406 (1971).
32. M. Munovitz and A. Pines, Adv. Chem. Phys. **6**, 1 (1987).
33. M. A. Lavrent'ev and B. V. Shabat, *Methods of Complex Analysis* (Nauka, Moscow, 1987), Chap. 7 [in Russian].
34. M. V. Fedoryuk, *Ordinary Differential Equations* (Nauka, Moscow, 1985), Chs. 3, 7 [in Russian].
35. A. A. Lundin and A. V. Makarenko, Sov. Phys. JETP **60**, 570 (1984).
36. A. A. Lundin, Sov. Phys. JETP **75**, 187 (1992).
37. M. Engelsberg and I. J. Lowe, Phys. Rev. B **10**, 822 (1974).
38. V. D. Fedotov and N. A. Abdrashitova, Vysokomol. Soedin. A **22**, 624 (1980).
39. R. E. Fornes, G. W. Parker, and I. D. Memory, Phys. Rev. B **1**, 4228 (1970).
40. B. T. Gravely and I. D. Memory, Phys. Rev. B **3**, 3426 (1971).
41. H. T. Stokes and D. C. Ailion, Phys. Rev. B **15**, 1271 (1977).
42. W. van der Lugt and W. J. Caspers, Phys. Rev. **30**, 1658 (1964).
43. P. Gaspard, in *Lecture Notes for the International Summer School, Fundamental Problems in Statistical Physics XI, Leuven, Belgium, 2005*, arXiv:cond-matter (2006).
44. P. Gaspard, in *Proceedings of the Symposium Henri Poincare*, Ed. by P. Gaspard, M. Henneaux, and F. Lambert (Int. Solvay Inst. Phys. Chem., Brussels, 2007), p. 97.
45. P. Gaspard, *Chaos, Scattering and Statistical Mechanics* (Cambridge Univ. Press, Cambridge, 1998).
46. V. L. Bodneva and A. A. Lundin, Theor. Math. Phys. **179**, 609 (2014).
47. D. Ruelle, Phys. Rev. Lett. **56**, 405 (1986).

Translated by V. Astakhov